## Responses to the Referee comments for #egusphere-2025-5544

The authors would like to thank the editor for handling our manuscript. We appreciate the insightful comments from the referees, which have helped improve the manuscript. Most of the revisions are minor and do not change the study's conclusions. The readability, clarity, and accuracy of the materials on Rossby wave theory and diagnostics have been improved thanks to the referees' comments.

Main changes are as follows:

1. Terminology: "Stationary Rossby Waves" changed to "Quasi-Stationary Rossby Waves" in most places (response to referee 2)
2. Method section: Substantially rewritten to improve precision and add context to the ray-tracing method and wave activity flux diagnostics (response to both referees).
3. Result section 3.3 (Model Biases in Rossby Wave Propagations) has been revised to include the stationary wavenumber $K_s$ and its physical interpretation (in response to both referees).
4. Appendix C has also been substantially edited to explain the stationary wavenumber and LZ15 ray tracing method in more detail (response to both referees).
5. Corrected inconsistencies in the notation and figure captions (response to both referees).

# Response to the referees

## Referee 1

The study proposes a novel framework for evaluation of the source of mean biases in surface air temperature affecting some dynamical downscaling approaches. The framework is based on process-level evaluation of stationary Rossby waves. The evaluation framework consists of a ray-tracing method which allows for a 2D basic state and the wave activity flux along with its divergence. The diagnostics are applied to simulations produced by two limited area models (RegCM4, WRF) and to a global variable-resolution model (CAM-MPAS). Evaluation of Rossby waves propagation shows that treatment of lateral boundary buffer zones can introduce discontinuities in the waves entering the model domain. Sensitivity experiments with WRF show that the no nudging spectral approach introduces spurious effects in the buffer zone. The authors show that errors in the simulation of stationary Rossby wave dynamics are related to mean biases in models. The study also includes an attempt to relate summer heatwaves to extreme wave activity.

The framework is an important tool to diagnose large-scale circulation simulated by dynamical downscaling approaches. The manuscript is well written and requires some minor revisions before acceptance.

**Reply**: We are glad to hear that you find the framework useful. Thank you very much for your positive comments as well as insightful feedback, which has improved the correctness and clarity of our manuscript.

### Comments on the downscaling methods

**Referee Comment 1.1.1** — CAM-MPAS is described as a non-hydrostatic model. Please add the type of dynamical core for the other two models.

**Reply**: We have added the following sentences describing the dynamical cores of each model in section 2.1.

"This model version solves the primitive (hydrostatic) equations on a $\sigma$ coordinate as described in Grell et al. (1994) and Elguindi et al. (2017)." (for RegCM4)

"The dynamical core solves the Euler equations without the hydrostatic assumption." (for WRF)

"... MPAS is a global dynamical core that solves the Euler equations on an unstructured grid (Skamarock et al., 2012)". (for CAM-MPAS)

**Referee Comment 1.1.2** — Page 7, paragraph 170: The reference to Appendix B1 describing the LB treatments should be provided here.

**Reply**: Thank you for the suggestion. We have added the reference to Appendix B1

" If this tenet is true, incoming Rossby wave signals are not affected by LBs or other model details (see Appendix B);..."

### Comments on Rossby wave ray theory

**Referee Comment 1.2.1** — Page 3, paragraph 235: add that 'k' is the zonal wave number and note that subscript 'g' refers to the wave group and not geostrophic flow $(u_g, v_g)$.

**Reply**: Thank you for the suggestions. We have added the two clarifications as:

"... where $k$ and $l$ are the zonal and meridional wavenumbers ($m^{-1}$), ..."
"The operators $d_g/dT = \partial/\partial T + u_g\partial/\partial X + v_g\partial/\partial Y$ represent the total derivative describing the rate of change following the wave packet moving at the group velocity (the subscript $g$ denotes *group*, not *geostrophic flow*)."

**Referee Comment 1.2.2** — Page 47, equation C1: define u and v. Paragraph 470: change 'single-level' to 'single-layer'.

**Reply**: After equation C1, we defined u and v as :
"...The friction is ignored. Also, with the assumption of a non-divergent system, $u$ and $v$ are the zonal and meridional components of rotational winds, respectively. "
Also, "single-level" has been changed to "single-layer":
" Strictly speaking, this single-layer (barotropic or shallow-water).... "

**Referee Comment 1.2.3** — Page 48: Equation C5 and C6: I think $\overline{\zeta}_a$ should be $\overline{\eta}$

**Reply**: Exactly, sorry for the typo. They have been corrected.

**Referee Comment 1.2.4** — Equation C10 does not imply that wavenumbers k and l depend on themselves. C10 tells that k and l are related through an implicit relationship that involves the mean state. The wavenumber can change due to wave-mean flow interactions but not because of wavenumbers depend on themselves. Please clarify whose time evolution depends on the number of waves and how this property relates to C10.

**Reply**: Thank you so much for this explanation. We have revised this section in Appendix C by adding the equations for the time rate of change of each wavenumber (equations C12 and C13), followed by the sentences revised as:
"... Equations C12 and C13 show that the base state wind shear changes the shape and scale of the wave (i.e., $k$ and $l$) as the wave travels at the group velocity."

**Referee Comment 1.2.5** — Page 49: Equations C11 and C13 replace $\eta_x$ and $\eta_y$ by $q_x$ and $q_y$. Please use a consistent notation, or define $q_x$ and $q_y$ if they have different meanings.

**Reply**: We have replaced $q_x$ and $q_y$ with $\eta_x$ and $\eta_y$. We also went through the entire text and figures to make sure the notation is consistent. Thank you for noting this inconsistency.

**Referee Comment 1.2.6** — Page 49: Please provide the physical interpretation of the stationary wavenumber Ks. Discuss what values Ks can take, what happens when nominator and denominator have positive and negative values.

**Reply**: Thanks for the suggestion. We have added a few paragraphs at the beginning of Section 3.3 to briefly explain the definition and physical interpretation of the stationary wavenumber $K_s$, along with

two new sub-figures in Figure 7 that show $K_s$ calculated from the ERA-Interim data in JJA. Appendix C1 is also expanded to provide more details to interested readers, including the suggested discussions.

The brief introduction of $K_s$ in the main text is as follows.

"... A commonly used diagnostic is the stationary wavenumber, $K_s$ (Hoskins and Karoly, 1981), which is derived from the dispersion relationship of Rossby waves under a zonally uniform state with zero meridional winds. The stationary wavenumber is defined as

$$K_s^2 = \frac{\overline{\eta}_y}{\overline{u}_M}.$$

It indicates where Rossby waves can propagate and where they are likely to be trapped or reflected; regions with real-valued $K_s$ are conducive to Rossby wave propagation, while those with imaginary $K_s$ are not. Over the regions where $K_s$ is real-valued, it acts as a cut-off filter for stationary waves. When $K_s$ is small (e.g., in strong westerlies), the total wavenumber allowed is low, so only very long waves can exist as stationary waves. Stationary wavenumber also acts like the refractive index for the optical wave solution, such that Rossby wave rays (paths of group velocity vectors) bend toward regions of higher $K_s$ [see Hoskins and Ambrizzi (1993), Li et al. (2018), and Appendix C.]"

The new paragraphs added in Appendix C1 (near the end of the section) are as follows.

"... In this simpler case, the total wavenumber depends on only two quantities: the meridional gradient of the background absolute vorticity and the background zonal wind. When either is negative, $K_s$ is an imaginary number. In this case, instead of oscillating in space, the wave solution becomes evanescent, decaying exponentially with distance (eqn. C7); hence, Rossby waves do not propagate over such a region.

For a zonally uniform background state, eqn C12 suggests $\frac{\partial \omega}{\partial X} = 0 = \frac{d_g k}{dT}$, so $k$ remains the same as given at the initial time $k_0$, while $l$ (hence $K_s$) evolves as the wavepacket travels through the background state. Changes in $l$ along the path are related to the meridional propagation of wave packets ($l$ is the y-component of the wavenumber vector, Fig. C1). Writing $l$ as:

$$l = \pm\sqrt{K_s^2 - k_0^2}$$

, we can see: 1) where $K_s$ is large and $K_s \gg k_0$, $l$ is real and large, thus Rossby waves can propagate meridionally with smaller meridional wavelengths, 2) where $K_s \approx k_0$, $l$ becomes small, the wave fronts become oriented North-South, and the wave energy travels almost purely zonally (Fig. C1b), and 3) where $K_s = k_0$, $l = 0$, and the wave cannot propagate any further meridionally, and turn back toward higher $K_s$ (turning latitude). If a Rossby wave is excited within the local maximum of $K_s$ with a sufficient latitudinal width, then the wave is trapped within the latitude band and propagates zonally since the strong gradients to the north and south refract back the waves.

In Fig. 7a, we apply this metric to each grid point, assuming that the metric $K_s$ is locally applicable; this is commonly done and able to provide a qualitative picture of the preferred wave pathways (Hoskins and Ambrizzi, 1993). An example of turning latitude is the north/south of the mid-latitude jet over the Pacific, where $K_s$ is becoming smaller toward the inhibited region. To the south of the subtropical jet, zonal winds are tending to zero, changing from westerly to easterly (Fig. 5a). This makes $K_s$ increase toward infinity, or the wavelength tends toward zero, implying that the waves break and mix into the background flow. Also, the group velocity decreases toward zero with increasing $K_s$ (eqn C15), thereby prohibiting wave propagation. This is called critical latitude."

### Comments on wave activity flux

**Referee Comment 1.3.1** — Page 11: In equation 3 bold fonts denote vector quantities; however, M, the wave activity density, is a scalar. Do not use a bold font for M.

**Reply**: Thanks for the clarification. M (as well as A and E) is changed to the standard font as:

$$\begin{aligned} \frac{\partial\, \mathrm{M}}{\partial t} + \nabla \cdot \mathbf{W} &= D_T \\ \mathrm{M} &= \frac{1}{2}(\mathrm{A} + \mathrm{E}) \end{aligned} \tag{1}$$

**Referee Comment 1.3.2** — Page 50: In equation C14 and the following paragraph, —V— denotes the magnitude of wind vector, thus a bold font must be used for V.

**Reply**: Thank you. We have corrected the font to boldface, using $|\mathbf{V}|$ instead of $|V|$.

**Referee Comment 1.3.3** — L285: This is not necessarily true. WAF can also be decomposed into different waves.

**Reply**: We are not quite sure what the referee means by "different waves", but to clarify, our original statement was about decomposing the WAF into contributions from different wave sources, which we think is difficult to do strictly, because WAF is a quadratic function of the perturbation field that includes interaction terms. Therefore, the WAF of a sum of two waves is not necessarily equal to the sum of the WAFs of each wave. However, we agree that it is possible to decompose the WAF into contributions from waves of different spatiotemporal scales by pre-processing the perturbation field, for example, with different filters. It is also straightforward to calculate WAF for waves with different phase speeds.

We have tested calculating WAFs from perturbation geopotential heights that are band-pass filtered with different frequencies with in the S2S scale (e.g., 5-25 days, 25-70 days, etc) and learned that, for specific cases (e.g., a strong El Nino year), WAFs with different time scales appear over different regions (e.g., those with shorter time scales over the Pacific, longer time scales over the Atlantic), thus revealing the dominant sources of WAF for different regions (not shown). However, we are not sure how we can decompose the WAF into contributions from different wave sources over climatological scales; for example, "on average in JJA over the western U.S., 30% of WAF comes from the North Pacific and 50% from the subtropical Eastern Pacific, and the rest from other regions.". We are keen to learn methods for this decomposition and would appreciate it if the referee could suggest methods or prior studies that have conducted such analyses.

With the above reasoning, we have revised the sentences in section 2.3.2 as follows.

"... we infer the source/sink of WA by the convergence/divergence of the horizontal components of the W-vector. With the complexity of realistic atmospheric fields, it can be challenging to identify the climatological sources of WA at a given location; one would need to systematically pre-process the perturbations to decompose Rossby waves into different spatiotemporal scales, or use idealized numerical experiments.

In this study, we apply a 25–90-day frequency band-pass filter to the perturbation geopotential height to extract the quasi-stationary Rossby wave signals. The phase velocity is set to zero in the W-vector terms (eqn. C19). ..."

### Comments on Climatology of large-scale circulation

**Referee Comment 1.4.1** — Page 13, paragraph 315: The mean bias figures (Fig. B1) show correctly no bias outside of the model domain for RegCAM4 and WRF, however, the analysis showing the ration of the standard deviation shows values different than 1 on these regions for both RegCAM4 and WRF. This result suggests that the frequency of data used in simulation is not the same as the frequency of the data used for verification. There are differences between Fig. 4c and Fig. 4d implying that the simulations also use ERA Interim data with different frequencies. This aspect needs some discussion.

**Reply**: Thank you for noting the difference in the raw data frequencies, which we missed. Indeed, the underlying sampling frequencies differ between ERA-Interim and model data. The former is available only at six-hourly intervals, which we used to calculate daily statistics, whereas the daily mean values from NA-CORDEX (and CAM-MPAS) are based on 3-hourly output. However, as shown below, we found that our result is not very sensitive to the difference.

First, please note that Fig. 4 in the main text shows only the inside of the regional model domain to focus on the temperature bias over land. On the other hand, Fig. B1 shows a larger area that extends beyond the regional model domains, with the ERA-Interim data patched in over those areas. In Fig.R1 below, we plotted the ratios of the standard deviations in the broader region as in Fig. B1. As you can see, the ratio is 1 outside the regional model domains (Fig R1c, d), just like the ratios of ERA-Interim data to itself (Fig R1a). Further outside is shown in white, because for this analysis on the monthly mean time series, we have extracted the data only over the North American continent (the shared region in Fig. R1a) from the global or the NA-CORDEX model data to save disk space and memory for calculation.

Additionally, Fig. R2a compares the JJA-mean tas calculated from the CAM-MPAS model's six-hourly and three-hourly outputs, denoted by $tas_{6hr}$ and $tas_{3hr}$, respectively. The difference in seasonal means is negligible relative to the model biases (we use the same color range as in the main figure), though it is nonzero. Similarly, Fig. R2b compares the standard deviations of monthly mean tas based on the six- and three-hourly data, as the ratio of standard deviations $tas_{6hr}/tas_{3hr}$. Again, the difference is negligible compared to the model bias using the same color range as Fig. 4. The largest difference is found near the Great Lakes (Fig. R2c), which is about 0.92 (or 0.08 difference), smaller by one magnitude than the actual model biases.

Based on these sensitivity tests, we added the following sentences in the main text, Section 2.2. (Data preparation):

"... According to the CORDEX protocol's model data requirements, daily mean quantities are calculated from three-hourly data (CORDEX, 2009). The CAM-MPAS data follow this requirement. The ERA-Interim data is available only every six hours, from which we calculated daily statistics. We compared the seasonal means and standard deviations of the monthly mean *tas* calculated from the six-hourly and three-hourly data, and found that the differences in these statistics are significantly smaller (less than 10 %) than the model biases against ERA-Interim (not shown)."

**Referee Comment 1.4.2** — Page 13, paragraph 325: 'seasonal to sub-seasonal' -¿ subseasonal to seasonal

**Reply**: The phrase has been corrected.

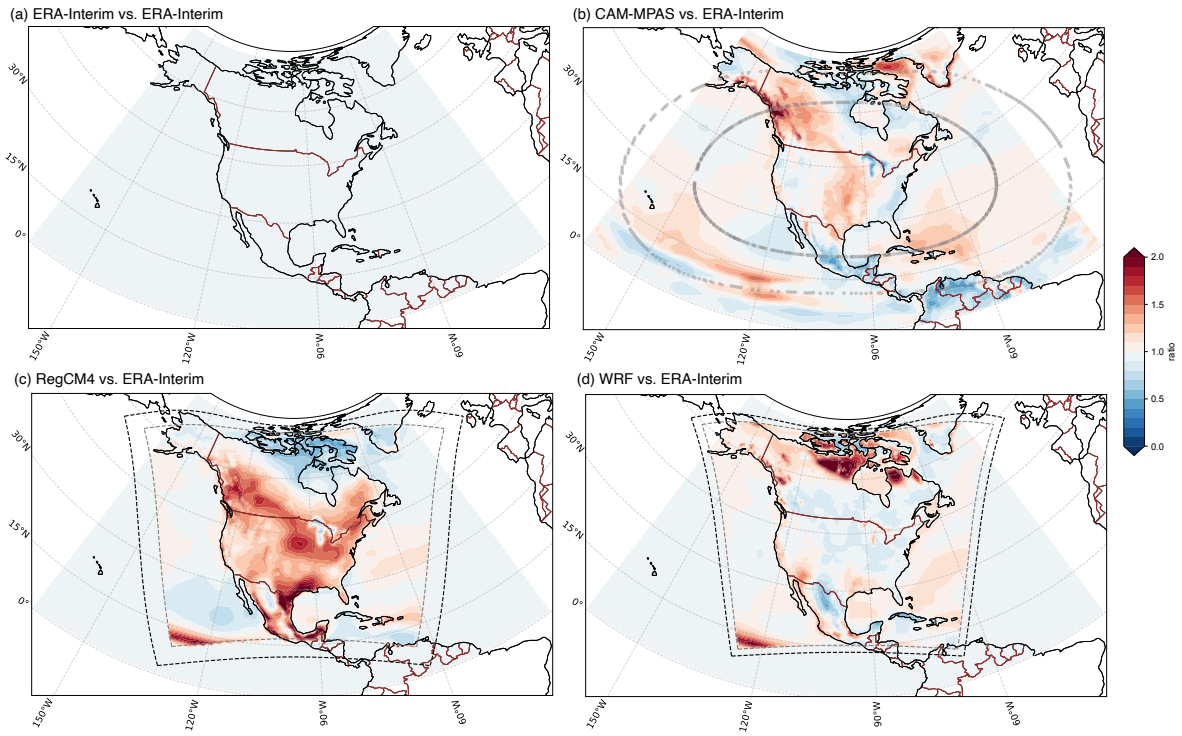


Figure R1: Same as Figure 4 (standard deviations of monthly mean surface air temperature divided by those of ERA-Interim) in the main text but showing a broader domain as in Figure B1: (a) ERA-Interim, (b) CAM-MPAS, (c) RegCM4, and (d) WRF.

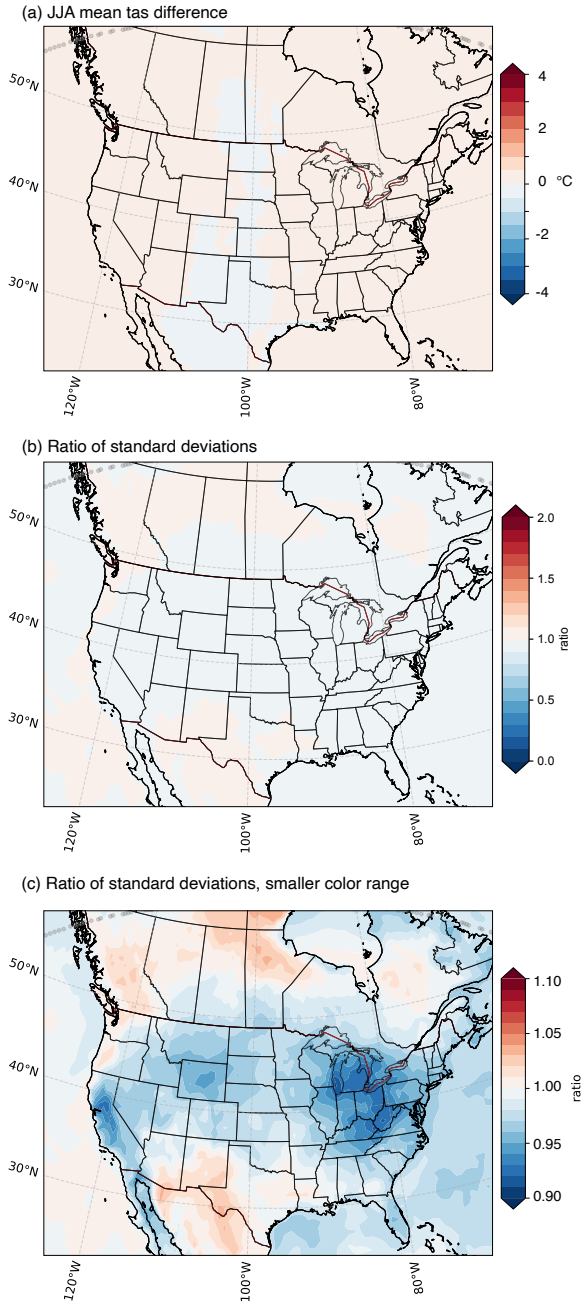


Figure R2: Sensitivity of monthly-mean (and seasonal climatology of) surface air temperature (tas) to the underlying data frequencies using the CAM-MPAS simulation output from 2000 to 2010. Panel (a) shows the difference of JJA mean tas calculated from the six-hourly data ($tas_{6hr}$) and that from the three-hourly data ($tas_{3hr}$), which was used in the main result. Panel (b) shows the ratio of the standard deviations of monthly mean tas based on the six- and three-hourly data, as $tas_{6hr}/tas_{3hr}$. Panel (c) is the same as (b) but using a much narrower color range for the filled contours.

### Comments on Model biases

**Referee Comment 1.5.1** — Page 20: The description of initial zonal wavenumber k in the figure caption is different from the values shown in each panel; in panel (a) initial $k = 2$ but the figure caption lists $k = 3$. In panel (b) initial $k = 4$ but the figure caption lists $k = 8$. Please clarify why these values are different. In the text, the initial wavenumber is denoted by $k_0$.

**Reply**: Thank you for noting the mistake in the figure caption. We have revised the caption to be consistent with the panel titles, using the same notation $k_0$ for the initial zonal wavenumber. We made sure to use the same notation $k_0$ in the text and other figure captions throughout the manuscript.

### Comments on Wave activity flux and surface air temperature

**Referee Comment 1.6.1** — Page 24, paragraph 460: the phase speed in the W terms is not mentioned either in Eq. 3 or in the Appendix C.

**Reply**: In the expression for the W-vector in Appendix C, we forgot the term representing the phase-speed contribution to the wave-activity flux. We have added the term in (now) eqn. C19.

### Comments on Rossby waves and heatwaves

**Referee Comment 1.7.1** — While this part is interesting, it would be a better contribution as a standalone study which will include a more in-depth analysis. Removing this part will make the length of the manuscript more manageable.

**Reply**: We agree with the referee that removing this part as a standalone study would make this manuscript more readable and concise, while the relationship between Rossby waves and heatwaves can be investigated in greater depth. However, we decided to keep this material mainly for a pragmatic reason: this study is supported by a project that aims to improve our understanding of extreme events. Meanwhile, we tried to shorten the main text by removing unnecessary sentences and moving some material to the Appendix (e.g., the former Figure 16, which shows the time series of extreme WA flux divergence). We also plan to revisit this question in a future study with a broader context that includes land-atmosphere interactions.

## Referee 2

This paper assess the ability of three different dynamical downscaling methodologies to simulate how quasi-stationary Rossby waves from remote regions lead to regional temperature anomalies and extremes over North America during summer. The three classes of models differ in how the large-scale forcing affects the downscaled domain: a LAM constrained only by lateral boundary conditions, a LAM with spectral nudging to maintain consistency in large-scale dynamics with the forcing data, and a global variable-resolution model with smoothly varying grid spacings. The model with spectral nudging is shown to perform best. The global variable resolution model suffers from time-mean biases in the upper-level circulation, leading to incorrect Rossby wave propagation. The LAM with just lateral boundary constraints also has biases in the large-scale flow and also abrupt changes in winds near the boundaries, again leading to incorrect Rossby wave propagation. Finally, the paper demonstrates that getting correct Rossby wave propagation and accumulation of wave activity is essential for surface temperature anomalies over the Southern Great Plains, an effect only captured with spectral nudging.

This was an interesting and well-written paper, and is well on its way to being suitable for publication. Nonetheless, I think the paper could be improved somewhat as described in my comments below. I should note that my background is in Rossby wave dynamics, and not in downscaling, which certainly is reflected in my comments below.

**Reply**: Thank you so much for your time and insightful comments, which help us improve our understanding on Rossby wave theory as well as the clarity and robustness of our analysis.

### Major comments: bandpass filter

**Referee Comment 2.1.1** — When the authors compute the WA fluxes, they apply a 25-90 day bandpass filter. Given that they are focused on the development of heat extremes on subweekly timescales, this seems to be too heavy of a filter. Specifically, because of this filter, the causality of the connections inferred in Figure 1 and in Figures 11-14 is somewhat ambiguous, as all of the changes should happen simultaneously if you filter out $< 25$ day variability. Are these results sensitive to this heavy filtering?

**Reply**: Thank you for the great question. Firstly, we want to clarify that while the band-passed WA flux contains signals only within the 25-90-day frequency range to focus on quasi-stationary waves, the geopotential height and surface air temperature anomalies in Figs. 11-14 are not filtered in the same way but are averaged using a 5-day moving window. Therefore, they contain all signals longer than five days, including those in the 25-90 day frequency range, which makes it reasonable to expect that the WA flux and the other variables are correlated. For heatwaves that typically last less than 25 days, the 25-90-day WF flux can be thought of as the slowly varying background forcing that modulates the probability of heatwaves.

We have removed the sentence that carelessly creates this ambiguity in the main text, which is "... Since the W-vector is calculated from the geopotential anomalies band-passed for 25-90 day variabilities, this assessment essentially examines correlations across time scales (5 days vs. 25-90 days) and across space between the West Coast and the rest of North America."

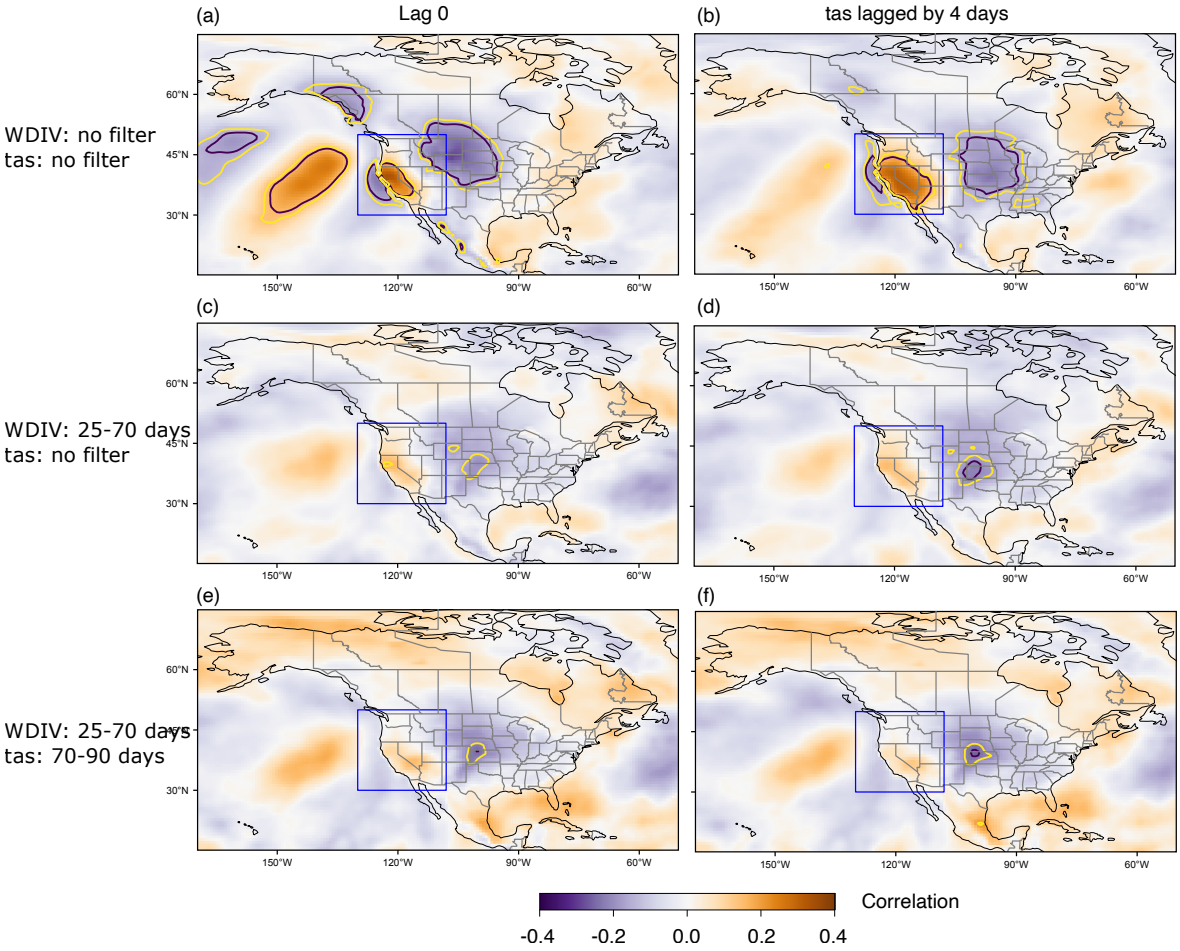


Figure R3: Same as Figure 13 in the main text [the lag-0 and lag-4 correlations between the W-vector divergence (WDIV) averaged over the West Coast (blue box) and surface temperature anomaly (tas) at each grid box] but with different time filters on each variable. All panels are based on the ERA-Interim data. The left column shows lag-0 correlation, and the right column shows the correlation with the tas time series lagged by 4 days. Each row shows different time filters: (a,b) no time filters applied to the two variables, but smoothed by five-day running mean, (c,d) W-vector is calculated from the geopotential height that is band-pass filtered for the 25-70 day period, and (e,f) the divergence of 25-70 day period W-vector and surface temperature anomalies band-passed for 70-90 day period.

Motivated by the referee's comment, we have also tested the sensitivity of the results to different filter frequencies of the geopotential height (which is used to calculate the W-vector) and surface air temperature (*tas*) anomalies: no filtering (but with a five-day running mean), 5-25 days, 25-70 days, and 70-90 days. The spatial patterns of the 30-year mean W-vector are similar across the different filters (not shown). The correlation results show interesting sensitivity to those different frequencies. Three examples are shown in Fig. R3. Without band-pass filters, and without any lags, correlation with statistical significance appears both upwind (over the Pacific) and downwind (U.S. Midwest) regions. (Fig. R3a). When *tas* is lagged by four days, then the significant correlations are found over the West Coast and over the U.S. Midwest only (Fig. R3b).

When a sub-seasonal (25-70) band-pass filter is applied only to the W-vector, then significant correlation is found over SGP, more strongly with lag+4 on *tas* (Fig. R3d), similar to Fig. 13 in the main text. This correlation is retained when a seasonal-scale (70-90 days) filter is applied to *tas* (Fig. R3f). Most other combinations of filters show no significant correlations (not shown).

The long, seasonal time scale of *tas* seems to involve long-term memory of soil and vegetation, which is expected to play an important role over SGP as one of the land-atmosphere coupling hotspots (e.g., Koster et al., 2004; Welty and Zeng, 2018). It may be that a few sub-seasonal peaks of the W-vector divergence are needed to slowly build a positive geopotential height perturbation and deplete soil moisture. We are not sure the physical significance of the lag of four days, given the long time scales of 25-70 and 70-90 day periods of the W-vector and *tas* anomalies involved. This interpretation is merely a hypothesis that needs to be tested and will be addressed in our future work. For this revision, we have added the following texts near Figure 13.

"... We noted that the significant lagged correlation remains when the *tas* anomaly is band-pass filtered for the periods between 70 and 90 days (not shown). The long timescale may indicate a role for the land surface, particularly soil moisture (e.g., Dirmeyer and Halder, 2017). The actual physical processes underlying the correlation are left for future work."

### Major comments: ray-tracing

I have a few questions about how ray-tracing is implemented here as compared to Hoskins and Karoly 1981.

**Referee Comment 2.2.1** — a. Equation 1: in classic ray tracing in Hoskins and Karoly 1981, k is kept constant. Why in the current formulism is it allowed to be a function of location? How much does k change as the wavetrain propagates away from the source region? More generally, please add a citation that derives equations 1 and 2.

**Reply**: A short answer to the first question ("Why in the current formalism is it allowed to be a function of location?") is because the basic state varies in zonal direction in the LZ15 formalism, i.e., $\frac{\partial}{\partial X} \neq 0$. For the third question ("please add a citation that derives equations 1 and 2"), we have added the references Whitham (1960) and Karoly (1983) to the particular sentence before the equations. The following is a long answer to the two questions, some of which have been added to Appendix C of the revised text.

LZ15 (first done by Karoly (1983)) applied the conservation of wavenumbers described by Whitham (1960) (their equation 9) to the basic state of the global atmosphere with non-zero, spatially varying zonal and meridional winds. Whitham (1960) showed that the wave field at a fixed point in space satisfies the relationship (1D example):

$$\frac{\partial k}{\partial t} + C_g \frac{\partial k}{\partial x} = -\frac{\partial \omega}{\partial x} \tag{2}$$

where

$$C_g = \frac{\partial \omega}{\partial k}$$

is the group velocity and $\omega$ is the frequency.

LZ15 applied the WKB method to this equation and wrote the left-hand side in terms of the total derivative following the group velocity ($D_g/dT$, using slowly varying coordinates T, X, and Y):

$$\frac{D_g k}{dT} = \frac{\partial k}{\partial T} + C_g \frac{\partial k}{\partial X}.$$

For the right-hand side of eqn. 2, we take the derivative of the dispersion relationship for the spatially varying background state [eqn. 7 of in Li et al. (2015) and eqn. 9 in Zhao et al. (2015)], which is:

$$\omega = \bar{u}k + \bar{v}l + \frac{\bar{\eta}_x l - \bar{\eta}_y k}{K^2}$$

For the zonal wavenumber $k$, we take the partial derivative of $\omega$ with respect to $X$:

$$\begin{aligned}\frac{\partial \omega}{\partial X} &= \frac{\partial}{\partial X}(\bar{u}k) + \frac{\partial}{\partial X}(\bar{v}l) + \frac{\partial}{\partial X}\left(\frac{\bar{\eta}_x l - \bar{\eta}_y k}{K^2}\right) \\ &= k\frac{\partial \bar{u}}{\partial X} + l\frac{\partial \bar{v}}{\partial X} + \frac{1}{K^2}\left(l\frac{\partial \bar{\eta}_x}{\partial X} - k\frac{\partial \bar{\eta}_y}{\partial X}\right)\end{aligned}$$

Substitute this back into the right-hand side of the ray tracing equation ($\frac{D_g k}{dt} = -\frac{\partial \omega}{\partial X}$), we get :

$$\frac{D_g k}{dt} = -\left[k\frac{\partial \bar{u}}{\partial X} + l\frac{\partial \bar{v}}{\partial X} + \frac{1}{K^2}\left(l\frac{\partial \bar{\eta}_x}{\partial X} - k\frac{\partial \bar{\eta}_y}{\partial X}\right)\right]$$

which is eqn. 11 in Li et al. (2015) and eqn. 12 in Zhao et al. (2015).

Without variations in the zonal direction, the right-hand size is zero; therefore, with a zonally uniform background state, $k$ stays constant. Zhao et al. (2015) shows in more detail how their formulation is reduced to that of Hoskins and Karoly (1981) with a zonally uniform, zero-meridional wind background state.

Lastly, for the second question ("How much does k change as the wavetrain propagates away from the source region?"), please look at the figure below (Fig. R4) showing examples of temporal evolution of zonal wavenumbers from our ray tracing using the ERA-Interim data. Li et al. (2015) shows the zonal and meridional wavenumbers in a variety of idealized background states in their Fig. 5. We did not include discussions on the wavenumber evolution in the main text to keep the manuscript length manageable.

**Referee Comment 2.2.2** — b. In line 290, the authors say that their implementation of ray tracing gives no information on the wave amplitude. While I can't say whether this is true of their implementation, it is clearly not true of the wave tracing WKB theory from Hoskins and Karoly, as they do diagnose wave amplitude. See their section 5. If the statement in line 290 is a typo and it is possible to infer wave amplitude, this would be an interesting addition to the (very long) paper

as it directly relates to heat extremes. If the statement in line 290 is correct, please explain why things are different from HK81.

**Reply**: The wave amplitude is not a part of the LZ15 framework mainly because the horizontally heterogeneous reference state with non-zero meridional winds makes the equation for the time evolution of wave amplitude very complex. It becomes a function of time, $y$ (latitude), and $x$ (longitude). Our understanding is that HK81 was able to analytically derive the amplitude equation by separation of variables [$(x,t)$ and $(y)$], with $k$ held constant, since the amplitude $P$ depends only on $y$ (their equation 5.18):

$$\psi' = P(y)e^{i(kx-\omega t)}$$

This is not the case with the assumed wave solution in LZ15:

$$\psi' = A(T,X,Y)e^{i(kx+ly-\omega t)}$$

where not only $l$ but also $k$ varies along the ray path as shown above. With this definition, the wave amplitude tendency equation becomes:

$$\begin{aligned}\frac{d_g A}{dT} = \Bigg[ &- \frac{1}{2K^2}\frac{d_g K^2}{dT} - \frac{1}{2}\left(\frac{\partial u_g}{\partial X} + \frac{\partial v_g}{\partial Y}\right) \\ &+ \frac{kl}{K^2}\left(\frac{\partial \bar{v}_M}{\partial X} + \frac{\partial \bar{u}_M}{\partial Y}\right) + \frac{k^2}{K^2}\frac{\partial \bar{u}_M}{\partial X} + \frac{l^2}{K^2}\frac{\partial \bar{v}_M}{\partial Y} - \frac{2\sin\varphi}{a}\bar{v}_M \Bigg] A\end{aligned} \tag{3}$$

where

$$\begin{aligned}\frac{1}{2K^2}\frac{d_g K^2}{dT} = &- \frac{1}{K^2}\left[k^2\frac{\partial \bar{u}_M}{\partial X} + kl\frac{\partial \bar{v}_M}{\partial X} + kl\frac{\partial \bar{u}_M}{\partial Y} + l^2\frac{\partial \bar{v}_M}{\partial Y}\right] \\ &- \frac{1}{K^4}\left[-k^2\frac{\partial \bar{q}_y}{\partial X} + kl\frac{\partial \bar{q}_x}{\partial X} - kl\frac{\partial \bar{q}_y}{\partial Y} + l^2\frac{\partial \bar{q}_x}{\partial Y}\right]\end{aligned} \tag{4}$$

and

$$\begin{aligned}\frac{\partial u_g}{\partial X} + \frac{\partial v_g}{\partial Y} = &\frac{\partial \bar{u}_M}{\partial X} + \frac{\partial \bar{v}_M}{\partial Y} \\ &+ \frac{1}{K^4}\left[(k^2-l^2)\frac{\partial \bar{q}_y}{\partial X} - 2kl\frac{\partial \bar{q}_x}{\partial X} + 2kl\frac{\partial \bar{q}_y}{\partial Y} + (k^2-l^2)\frac{\partial \bar{q}_y}{\partial Y}\right]\end{aligned} \tag{5}$$

In addition to the complicated form of the amplitude tendency equation, unlike wavenumbers that have algebraic constraints from the dispersion relationship along the ray path, the wave amplitude does not have such constraints and depends on the history of the ray path, and therefore, it is not straightforward to solve for the amplitude along the ray path as errors accumulate.

Another approach would be to use a conserved quantity along the ray path, such as wave action density, to infer the wave amplitude, as used by HK81 to confirm their results. However, the wave

action density and its variants are not locally/strictly conserved (e.g., Huang and Nakamura, 2017; Wang et al., 2021) where the reference state varies rapidly, and/or in the presence of strong non-conservative processes (e.g., diabatic heating), as also mentioned in the TN01 paper. Although TN01 shows that the time tendency of their wave activity density generally matches the wave activity flux convergence, we can see some non-negligible residuals locally (Their Figs. 8c and 9c). We consider this tolerable for snapshot diagnostics with the TN01 framework, averaged over 30 years of JJA days, given our focus on model evaluation. But it may not be suitable for diagnosing the wave amplitude along the ray path.

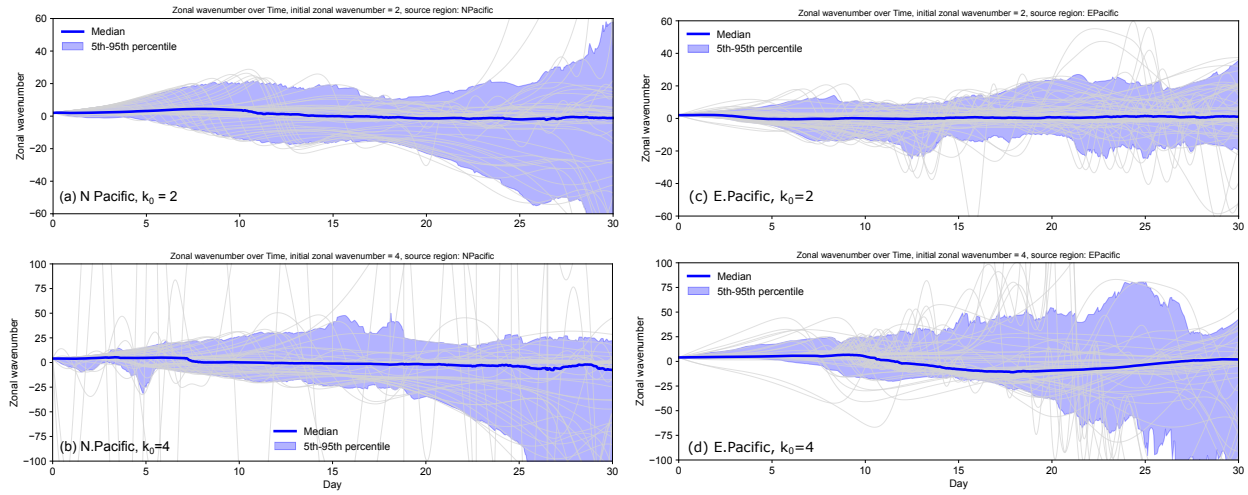


Figure R4: Time evolution of the zonal wavenumber $k$ along the ray path for the top four panels shown in Fig. 8 in the main text: (a, b) the rays from the North Pacific source with initial zonal wavenumber $k_0 = 2$ and $k_0 = 4$, and (c, d) the rays from the East Pacific source with $k_0 = 2$ and $k_0 = 4$. The x-axis is time in days, and the y-axis is the zonal wavenumber. The thick line is the median of the 200 (264 for the East Pacific source) ray paths, and the shaded area is the 5th-95th percentile range. Think of gray lines as subsampled individual ray paths (every 4 source grid points).

## Minor comments

**Referee Comment 2.3.1** — 1. The paper refers to these wavetrains propagating into North America on subseasonal timscales as stationary Rossby waves. I think a more suitable terminology is "quasi-stationary Rossby waves", as typically stationary waves are averaged over an entire season (or at least over an entire month). See e.g., White et al.

**Reply**: Thank you for the clarification and helpful reference. We have updated the terminology to "quasi-stationary Rossby waves" in most instances. For those citing previous work that used "stationary waves", we have kept the original terminology.

**Referee Comment 2.3.2** — 2. Line 31: the sentence "Since phase speed is inversely proportional to wavenumber, larger waves tend to have greater phase speed." Is an oversimplification, and depending on how it's interpreted incorrect. I suggest deleting.

**Reply**: We have deleted the sentence as recommended.

**Referee Comment 2.3.3** — 3. Line 342: "creates" isn't precise. It seeds relative vorticity, but doesn't create any vorticity per se.

**Reply**: I see, thank you for the clarification. We have revised the sentence as follows "... Also, the interaction between vorticity and divergence alters the local vorticity balance (via vortex stretching, $-\eta(\nabla \cdot \mathbf{v})$), acting as a source of relative vorticity anomalies, often called Rossby Wave Sources (RWS) ...".

**Referee Comment 2.3.4** — 4. Figure 8-10 demonstrate that there exists a waveguide in the climatological circulation (e.g., a North Pacific subpolar waveguide appears to trap $k = 6$ or $k = 8$). Previous work has diagnosed such a waveguide using $K_s$ (as the authors later note), and while $K_s$ has many suspect assumptions underlying it, it is a more intuitive tool than the more comprehensive but black-boxy tools used in this paper. If my intuition is correct and there is a waveguide formed via a $K_s$ local extrema, I think the paper would be clearer if this was shown explicitly.

**Reply**: Thank you so much for the suggestion. We have included figure panels showing $K_s$ in Fig. 8 to demonstrate that the main waveguides can be identified by $K_s$, consistent with the other two diagnostics. We feel starting this section with $K_s$ makes more logical sense. We also illustrated three differences between $K_s$ and the other diagnostics: southward propagation over the central Pacific, northeastward propagation along the subtropical jet, and northward propagation off the West Coast of North America, which are not clearly indicated by $K_s$. We have also added an explanation of $K_s$ at the beginning of subsection 3.3 and also in Appendix C.

**Referee Comment 2.3.5** — 5. Figure 8: please fix the panel titles. Also, the caption doesn't appear to accurately reflect the figure contents.

**Reply**: Sorry for the confusing labels and captions. We have fixed the panel titles and updated the caption to accurately reflect the figure contents.

**Referee Comment 2.3.6** — 6. Line 433: **to** travel north

**Reply**: Thank you, it's been corrected.

**Referee Comment 2.3.7** — 7. Equation C11 and C13. The authors jump from $\eta_y$ and $\eta_x$ to $q_x$ and $q_y$. I assume this is just a notational issue, as the authors are neglecting stretching vorticity/divergence. If yes, please keep the original notation.

**Reply**: Yes, it was a notational mistake. We have corrected $q_x$ and $q_y$ to $\eta_y$ and $\eta_x$.

## References


Dirmeyer, P. A. and Halder, S.: Application of the Land–Atmosphere Coupling Paradigm to the Operational Coupled Forecast System, Version 2 (CFSv2), Journal of Hydrometeorology, 18, 85–108, https://doi.org/10.1175/JHM-D-16-0064.1, 2017.

Elguindi, N., Bi, X., Giorgi, F., Nagarajan, B., Pal, J. S., Solmon, F., Rauscher, S. A., Zakey, A., O'Brien, T. A., Nogherotto, R., and Giuliani, G.: Regional Climate Model RegCM Reference Manual Version 4.7, Tech. rep., The Abdus Salam International Centre for Theoretical Physics, Trieste, Italy, issue: January, 2017.

Grell, G. A., Dudhia, J., and Stauffer, D. R.: A description of the fifth-generation Penn State/NCAR Mesoscale Model (MM5), Tech. rep., University Corporation for Atmospheric Research, Boulder, CO, ISSN 00424625, https://doi.org/10.5065/D60Z716B, publication Title: NCAR/TN-398+STR Volume: 115 Issue: 10, 1994.

Hoskins, B. J. and Karoly, D. J.: The steady linear response of a spherical atmosphere to thermal and orographic forcing, Journal of the Atmospheric Sciences, 38, 1179–1196, `http://journals.ametsoc.org/doi/abs/10.1175/1520-0469(1981)038<1179:TSLROA>2.0.CO;2`, 1981.

Huang, C. S. Y. and Nakamura, N.: Local wave activity budgets of the wintertime Northern Hemisphere: Implication for the Pacific and Atlantic storm tracks, Geophysical Research Letters, 44, 5673–5682, https://doi.org/10.1002/2017GL073760, _eprint: https://onlinelibrary.wiley.com/doi/pdf/10.1002/2017GL073760, 2017.

Karoly, D. J.: Rossby wave propagation in a barotropic atmosphere, Dynamics of Atmospheres and Oceans, 7, 111–125, https://doi.org/10.1016/0377-0265(83)90013-1, 1983.

Koster, R. D., Dirmeyer, P. A., Guo, Z., Bonan, G., Chan, E., Cox, P., Gordon, C. T., Kanae, S., Kowalczyk, E., Lawrence, D., Liu, P., Lu, C.-H. H., Malyshev, S., McAvaney, B., Mitchell, K., Mocko, D., Oki, T., Oleson, K., Pitman, A., Sud, Y. C., Taylor, C. M., Verseghy, D., Vasic, R., Xue, Y., and Yamada, T.: Regions of strong coupling between soil moisture and precipitation., Science (New York, N.Y.), 305, 1138–40, https://doi.org/10.1126/science.1100217, 2004.

Li, Y., Li, J., Jin, F. F., and Zhao, S.: Interhemispheric propagation of stationary rossby waves in a horizontally nonuniform background flow, Journal of the Atmospheric Sciences, 72, 3233–3256, https://doi.org/10.1175/JAS-D-14-0239.1, 2015.

Skamarock, W. C., Klemp, J. B., Duda, M. G., Fowler, L. D., Park, S.-H., and Ringler, T. D.: A multiscale nonhydrostatic atmospheric model using Centroidal Voronoi Tesselations and C-grid staggering, Monthly Weather Review, 140, 3090–3105, https://doi.org/10.1175/MWR-D-11-00215.1, 2012.

Wang, M., Zhang, Y., and Lu, J.: The Evolution Dynamical Processes of Ural Blocking Through the Lens of Local Finite-Amplitude Wave Activity Budget Analysis, Geophysical Research Letters, 48, e2020GL091 727, https://doi.org/10.1029/2020GL091727, _eprint: https://agupubs.onlinelibrary.wiley.com/doi/pdf/10.1029/2020GL091727, 2021.

Welty, J. and Zeng, X.: Does Soil Moisture Affect Warm Season Precipitation Over the Southern Great Plains?, Geophysical Research Letters, 45, 7866–7873, https://doi.org/10.1029/2018GL078598, 2018.

Whitham, G. B.: A note on group velocity, Journal of Fluid Mechanics, 9, 347–352, https://doi.org/10.1017/S0022112060001158, 1960.

Zhao, S., Li, J., and Li, Y.: Dynamics of an interhemispheric teleconnection across the critical latitude through a southerly duct during boreal winter, Journal of Climate, 28, 7437–7456, https://doi.org/10.1175/JCLI-D-14-00425.1, 2015.